Available online at www.sciencedirect.com
ScienceDirect
Trans. Nonferrous Met. Soc. China 35(2025) 3714−3733
Transactions of Nonferrous Metals Society of China
www.tnmsc.cn

Heterogeneous globularization in lamellar-structured Ti−6Al−4V alloy by heavy warm rolling and annealing treatment

Xiao-feng WU[1], Li-ming FU[1,2,3], Shuo MA[1,2], Ai-dang SHAN[1,2,3]

1. School of Materials Science and Engineering, Shanghai Jiao Tong University, Shanghai 200240, China;
2. Shanghai Key Laboratory of High Temperature Materials and Precision Forming, Shanghai Jiao Tong University, Shanghai 200240, China;
3. Collaborative Innovation Center for Advanced Ship and Deep-Sea Exploration, Shanghai 200240, China

Received 1 March 2024; accepted 17 December 2024

Abstract: The impact of rolling temperature and the crystallographic orientation of α-colonies on the globularization behavior of lamellar α+β microstructure in Ti−6Al−4V alloy was investigated. Firstly, the lamellar structure was heavily rolled at 600, 700, 800 and 900 °C, respectively. Heavy rolling from temperatures of 600 to 900 °C resulted in an increased volume fraction and thickness of β lamellae, while the corresponding parameters for α lamellae decreased. Then, these rolled α+β lamellar microstructures were spheroidized into equiaxed grains upon subsequent annealing. The results demonstrate that the globularization fraction of the lamellar structures diminishes as the rolling temperature increases. Additionally, the globularization fraction for α-colonies with hard crystallographic orientations, such as ⟨0001⟩//ND and ⟨0001⟩//TD, is considerably lower compared to those with softer orientations, positioned at certain angles to ND, RD, and TD during annealing process. This results in heterogeneous globularization of α lamellae, leading to the development of pronounced sharp micro-texture. Furthermore, the slipping deformations of α-colonies with varying crystallographic orientations during rolling were meticulously analyzed.

Key words: heterogeneous globularization; Ti−6Al−4V alloy; lamellar structure; slip; orientation; misorientation

1 Introduction

Titanium alloy has gradually adapted to the development of energy conservation, emission reduction, environmental protection in current society because of its specific strength, stiffness and excellent corrosion resistance properties. Ti−6Al−4V alloy is a typical two-phase titanium alloy, composed of α phase with hcp crystal structure ($P6_3mmc$) and β phase with bcc crystal structure ($Im3m$) at room temperature. Since this alloy contains a few stable β phase elements (V, Mo, Nb, Fe, etc), its microstructure consists of about 93% of α phase and 7% of β phase by volume [1,2]. The as-cast Ti−6Al−4V alloy is usually deformed in the high-temperature β phase zone to reduce casting defects such as cavitation and shrinkage. During subsequent slow cooling, α lamellae with different orientations called α-colony form within the coarse β-phase grains, and maintain the Burgers orientation relationship (BOR) with parent β phase [2]. The thick α lamellae, together with untransformed thin β lamellae, consist of the typical α+β lamellar structure, which is detrimental to ambient mechanical properties. Therefore, secondary thermo-mechanical processing was used to treat the α+β lamellar structure into equiaxed α-grains.

Corresponding author: Li-ming FU, Tel: +86-21-54748974, Fax: 86-21-54740825, E-mail: lmfu@sjtu.edu.cn;
Ai-dang SHAN, Tel: +86-21-54747556, Fax: 86-21-54740825, E-mail: adshan@sjtu.edu.cn
https://doi.org/10.1016/S1003-6326(25)66908-1

The thick α lamellae will undergo a series of microstructure evolution, such as α-colonies kinked, α lamellae globularization/recrystallization during the secondary thermo-mechanical processing (STMP). The different α-colonies with various orientations will inevitably lead to different stress statuses during STMP. Regarding the micro-crystal structure, the activation of the slip system in hcp crystal cell is different for various orientation α-colonies, which leads to the micro-zone formation and heterogeneous mechanical properties. Therefore, understanding the microstructure evolution of α lamellae in thermo-mechanical processing is of great significance for regulating different mechanical properties. Previous studies [3,4] revealed that α lamellae paralleled to the pressure direction tend to kink during thermal deformation. The orientation of the kinked α lamellae is always "hard", while the other α-colonies owning "soft" orientation forms band-shaped tissue along the deformation direction. Compared with the other titanium alloys with equiaxed structures, the large α-colonies lead to heterogeneous deformation and plastic instability in the lamellar microstructure during the thermo-mechanical processing. JIANG et al [5] proposed that micro shear bands often arise as a typical instability phenomenon due to the various orientations of α-colony. Moreover, the original BOR relationship between α and β phase is destroyed during deformation. JIA et al [6] reported that the kinking of α lamellae requires a critical deformation degree. The α lamellae begin to kink when the equivalent strain ε reaches 0.3, and the deformation temperature is 800 °C. With the deformation increase, α lamellae will be globularized and convert to equiaxed α phase and SEMIATIN [7]. The globularization behavior of α lamellae is associated with the crystalline orientation of different α-colonies. The more c axis aligns to the force axis, the larger the Taylor factor, α lamella is more difficult to deform, and the globularization is more sluggish. Moreover, the crystal orientation of α-colony is also closely related to the texture of the parent phase β phase [8]. The spheroidization of α lamellar structure is always related to the strain rate. The smaller the strain rate is, the more favorable the globularization is [9]. Some studies also believe that the globularization of lamellar structure is related to crystal orientation, and consider that the globularization of α-colony is closely associated with its size [10,11]. Due to the poor symmetry of the hexagonal close-packed (hcp) lattice structure, the orientation of the lamellar structure will directly affect the deformation mode of the hcp unit crystal. In term of pure titanium and titanium alloy, the first slip system for hcp is prismatic slip and basal slip, the prismatic slip is preferentially activated, and pyramidal slip is difficult to active at room temperature due to its high CRSS and large Burger vector [12−16]. Most previous studies were concentrated on the microstructure evolution of α lamellae at a lower (α+β) regime during thermal deformation. In contrast, the studies related to subsequent annealing effect on deformed α lamellae and rolling deformation behavior of various α-colonies are relatively less. Thus, understanding the microstructure evolution of α lamellae during warm-rolling deformation and annealing and its connection to the micro-texture formation is vital.

Whereas substantial research has explored the microstructural evolution and deformation behavior during warm rolling, literature offering a comprehensive explanation, particularly at high reduction ratios (exceeding 80%), remains sparse. This study applied heavy warm rolling with a total reduction rate of up to 93%, to transform the α+β lamellar structure into equiaxed grains. We aim to establish a detailed relationship between the orientation of α-colonies and the microstructure evolution of post-rolling and annealing. Furthermore, we will elucidate the impact of rolling temperature on the efficiency of globularization, providing insights that could significantly enhance material processing techniques.

2 Experimental

2.1 Material and processing

The base material used in this study was Ti−6Al−4V alloy, characterized by a chemical composition of 5.6 wt.% Al, 4.2 wt.% V, and balance Ti. The β transus temperature of this alloy is approximately 995 °C, as reported in prior studies [2]. Rectangular plates, each measuring 50 mm × mm 50 mm × 30 mm, were prepared from the as-received alloy using wire-electrode cutting. These plates underwent a pre-rolling heat treatment at different temperatures (600, 700, 800, and 900 °C) for 10 min to ensure uniform heating

throughout the samples.

Following heat treatment, the plates were subjected to a warm heavy rolling process, achieving a reduction rate of 93% over 6 passes. Immediately, after rolling, the strips were quenched in water to preserve the deformed microstructure. Subsequently, the strips underwent an annealing treatment to further refine the microstructure. The details of these processes are depicted in Table 1 and Fig. 1.

2.2 Microstructural characterization by SEM

Microstructural analysis of the rolled and annealed Ti−6Al−4V specimens was performed on the ND−RD plane. Specimen preparation involved metallographic polishing followed by etching for 30 s using an etchant composed of 5 vol.% hydrofluoric acid (HF), 10 vol.% nitric acid (HNO_3), and 85 vol.% water. Micrographs were obtained using a TESCAN MIRA3 scanning electron microscope (SEM) equipped with electron backscatter diffraction (EBSD) detectors. The microstructural features were quantitatively analyzed using the standard linear intercept method, with calculations performed using Image-Pro Plus software. Globularization initiation was rationalized with an aspect ratio of less than 2:1, and the aspect ratio is calculated by the horizontal length and the vertical thickness of α lamellae [11]. Several SEM micrographs were analyzed to ensure the measurement accuracy.

2.3 Microstructural characterization by EBSD

The orientation of the annealed specimens was characterized using the electron backscatter diffraction (EBSD) technique. For EBSD analysis, specimens were electro-polished using an electrolyte composed of 600 mL methanol, 360 mL oxyethanol, and 60 mL perchloric acid. The analysis was performed at an acceleration voltage

Table 1 Rolling schedule of Ti−6Al−4V alloy

Rooling temperature/ °C	Starting thickness/ mm	Final thickness/ mm	Holding time and temperature	Rolled alloy	Annealing temperature and time	Annealed alloy
600	30	2	10 min, 600 °C	R600	700 °C, 1 h	RA600
700	30	2	10 min, 700 °C	R700	700 °C, 1 h	RA700
800	30	2	10 min, 800 °C	R800	700 °C, 1 h	RA800
900	30	2	10 min, 900 °C	R900	700 °C, 1 h	RA900

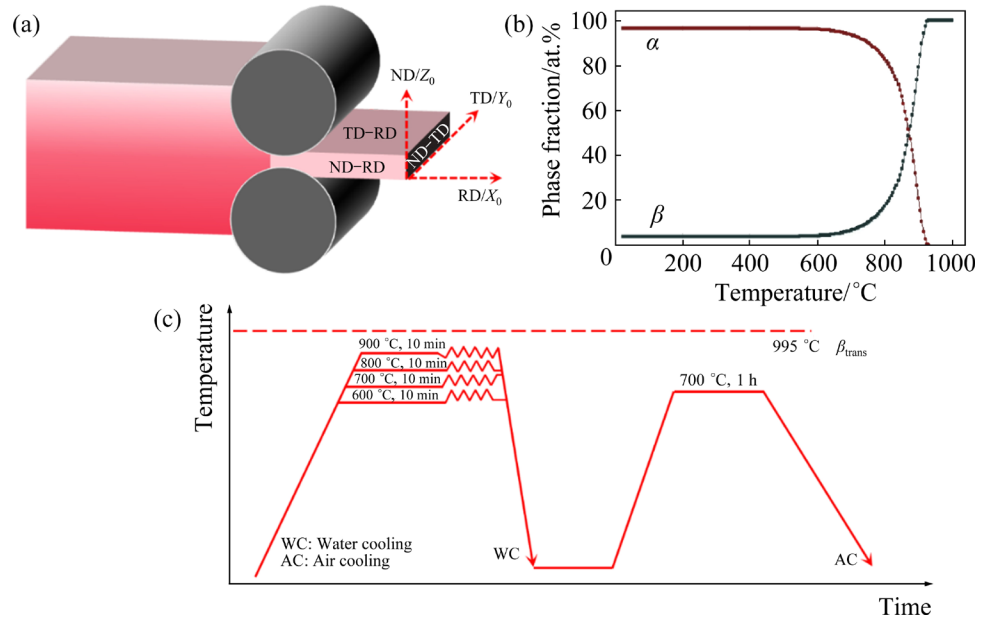

Fig. 1 Illustration of three directions corresponding to rolled sample (a); Equilibrium phase diagram calculated by JamtPro software (b); Schematic diagram of heavy warm rolling process (c)

of 15 kV, with a scanning step size of 100 nm across a scanning area of 80 μm × 80 μm. EBSD data were processed using Channel-5 software. Grain boundaries were categorized based on their misorientation: boundaries with a misorientation between 2° and 10° were defined as low-angle grain boundaries (LABs) and outlined in blue, while high-angle grain boundaries (HABs) with a misorientation exceeding 10° were outlined in black.

2.4 XRD analysis

X-ray diffraction (XRD) experiments were carried out using a Shimadzu XRD−6000 diffractometer equipped with Cu K_α radiation. The system was operated at an acceleration voltage of 40 kV and a current of 40 mA. Measurements covered an angular range from 30° to 90°, with a step size of 0.02° and a counting time of 2 s per step. For the dislocation density analysis, a multiple whole-profile fitting procedure was employed to examine the XRD line profiles, taking into account the influence of the diffraction vector and Burgers vectors. It is noted that in the hexagonal close-packed (hcp) lattice structure, there are primarily three types of Burgers vectors: $\langle a_\alpha \rangle$, $\langle c_\alpha \rangle$, and $\langle c_\alpha + a_\alpha \rangle$. This study assumed a random distribution of a specific Burgers vector type across different slip systems to simplify the calculation. For the β-phase, which features a body-centered cubic (bcc) lattice structure, the dislocation density calculation employed the modified Williamson-Hall method, focusing on conventional $\alpha_\beta/2\langle 111 \rangle$ dislocations [12−16].

3 Results

3.1 Microstructure evolution

The microstructure of the as-received Ti−6Al−4V alloy features Widmanstätten α-colonies, comprising thick α lamellae and thin β-phase lamellae. The prior β grain size varies from tens to hundreds of microns, while α-colonies, which form at β grain boundaries or within β grains, range in size up to 10 μm. The α lamellae are 5−10 μm in thickness, whereas the residual β lamellae are several tens of nanometers thick. Figures 2(a−c) illustrate that the α-phase, with its hexagonal close-packed (hcp) crystal structure, appears darker, whereas the β-phase, with a body-centered cubic (bcc) crystal structure, appears lighter. This observation is corroborated by XRD results, which confirm the predominance of the α-phase in the SEM microstructure. Additionally, Fig. 2(e) shows that the α lamellae maintain a Burgers orientation relationship (BOR) with the parent β phase, characterized as $(0001)_\alpha // (110)_\beta$ and $[2\bar{1}\bar{1}0]_\alpha // [\bar{1}11]_\beta$ [8,9]. Figure 2(d) indicates that α-colonies exhibit various orientations and sizes, ranging from a few to tens of micrometers.

During the rolling process, α-colonies with varying orientations exhibit distinct microstructural evolutions. As illustrated in Figs. 3(a1, a2), micro shear bands highlighted with a yellow line, developed in localized areas at a temperature of 600 °C (R600). These bands are particularly associated with orientations that are resistant to deformation (termed as “hard orientation”). The formation of micro shear bands facilitates the coordination of deformation across different α-colonies. Notably, these bands appear darker than the surrounding microstructure in etched samples, which suggests increased susceptibility to corrosion [5].

Figure 4 shows that as the rolling temperature increases, the thickness of α lamellae remains relatively unchanged, whereas the thickness of β lamellae increases. Figures 3(b1, b2, c1, c2, d1, d2) (within the yellow dotted line) demonstrate that α lamellae perpendicular to the rolling direction (RD) tend to kink. However, most α lamellae rotate to eventually align parallel to the RD, which benefits to reducing microstructural heterogeneity between adjacent α-colonies. The application of water-cooling was intended to preserve the rolled microstructure, consequently inhibiting the globularization of α lamellae. During the subsequent annealing process, significant microstructural transformations occur, including the fracturing of β lamellae and the globularization of α lamellae. It is important to note that, globularization is used in a broad sense and is not considered mutually exclusive from recrystallization. Moreover, numerous secondary nano β_{II} phase particles precipitate from the α lamellae, as depicted in Figs. 3(a3, b3, c3, d3). The size of these β_{II} phase nanoparticles ranges from a few to tens of nanometers.

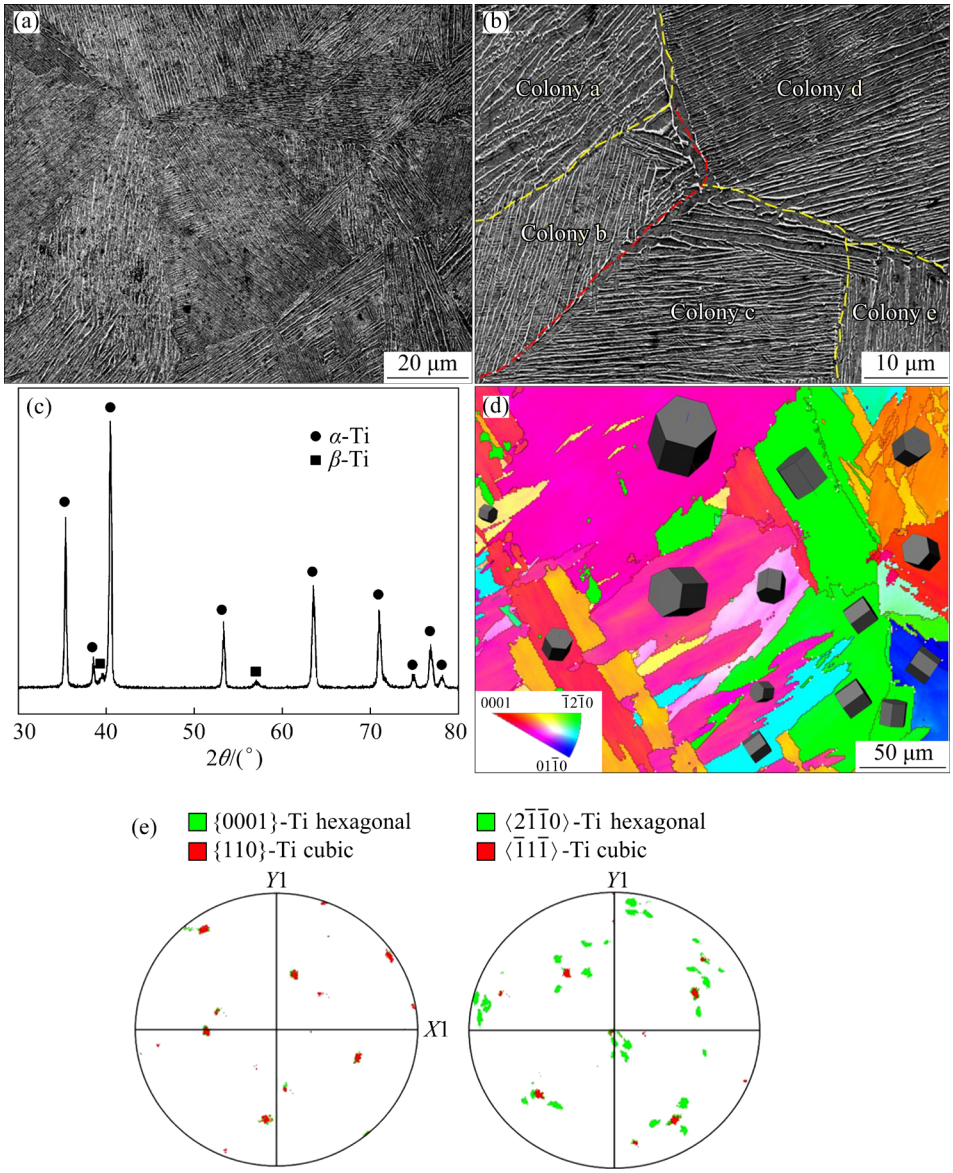

Fig. 2 SEM images of α-colony (a, b), XRD pattern of as-received alloy (c), IPF map of as-received alloy (d), and orientation relationship between α and β phases based on parent grain reconstruction (e)

The annealed microstructures reveal varying degrees of α-colonies globularization depending on their crystallographic orientations. Meanwhile, Fig. 4 indicates that the globularization fraction decreases with increasing rolling temperature. For RA600 and RA700 samples, most of the β lamellae fragment into small particles, while α lamellae transform into equiaxed grains. However, in certain local microstructures, as highlighted by the yellow dotted lines in Figs. 5(b3, c3, d3), remnant α lamellae with high aspect ratios remain prevalent. In these areas, β lamellae partially penetrate the α lamellae, forming grooves [10]. SHARMA et al [11] suggested that this penetration of the β phase generally initiates the globularization of α lamellae, a process that continues until the α lamellae become equiaxed grains [11]. Previous research [1,12,13] has identified four principal mechanisms for α lamella globularization: recrystallization, boundary splitting, shearing mechanism, and termination migration. Termination migration, involving atom diffusion, typically requires a long annealing period. Given the rapid water cooling applied in this study to preserve the rolled microstructure and the short annealing duration, termination migration is considered to be less effective compared to the other three mechanisms. In contrast, for RA800 and RA900 samples, the prevalence of α-colonies retaining lamellae with a high aspect ratio is more pronounced.

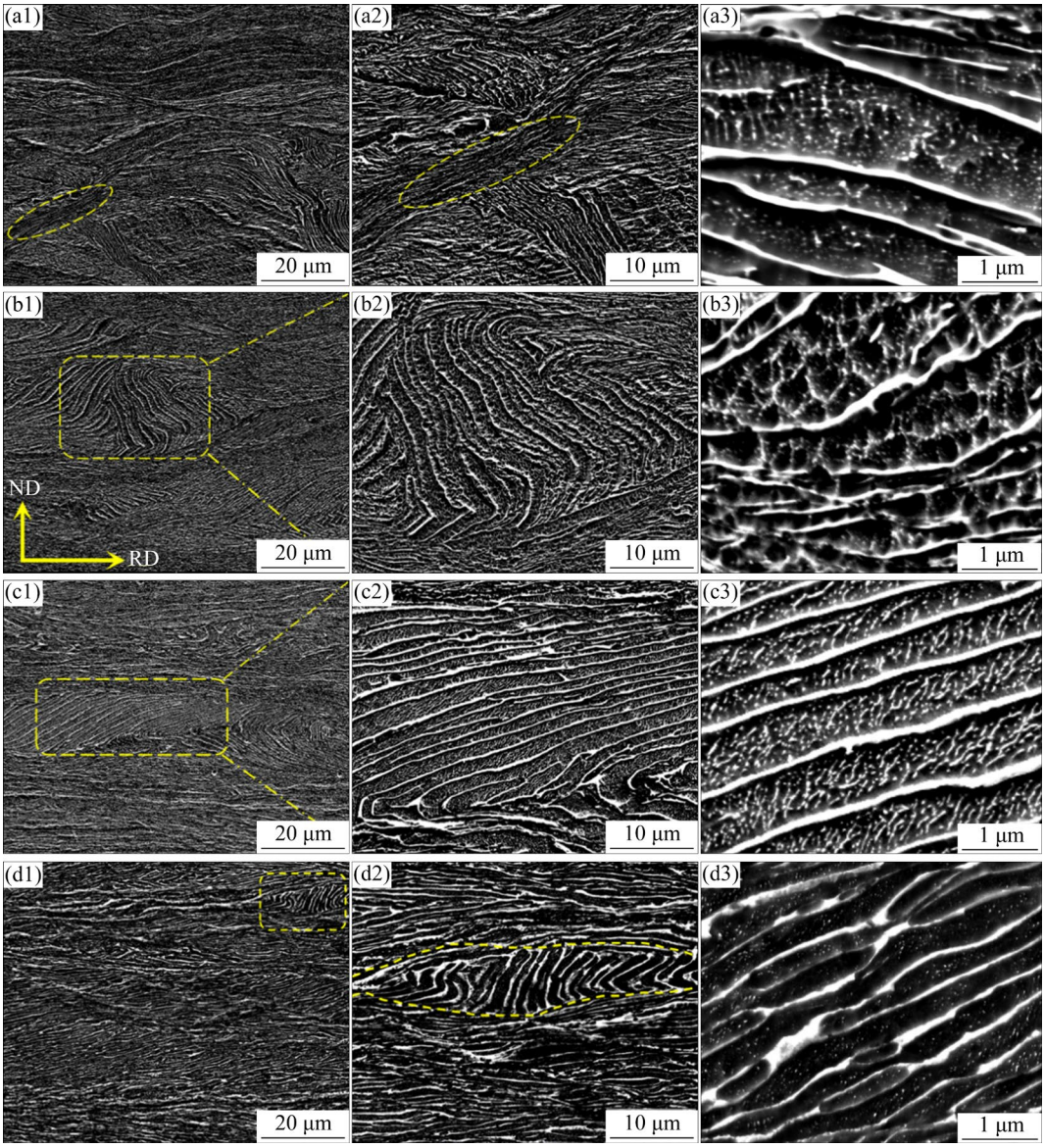

Fig. 3 SEM images of rolled samples: (a1, a2, a3) R600; (b1, b2, b3) R700; (c1, c2, c3) R800; (d1, d2, d3) R900

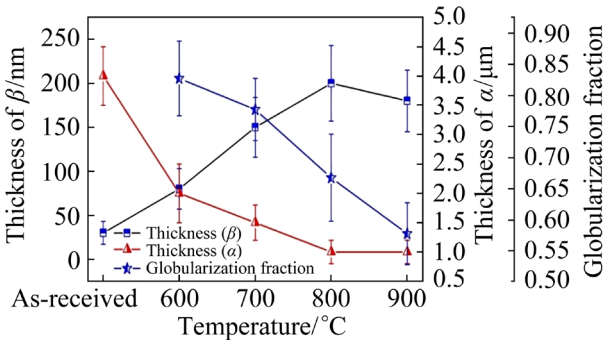

Fig. 4 Effect of rolling temperature on thickness of α, β lamellae and globularization fraction for α lamellae

The degree of globularization for straight α lamellae that are parallel to the rolling direction (RD), is typically greater than that of the kinked α lamellae. As illustrated in Figs. 5(d2, d3), the kinked α-colonies (outside of the yellow dotted line) retain their lamellar morphology; however, within the micro shear bands marked by the yellow dotted lines, the α lamellae have transformed into equiaxed grains. These micro shear bands, indicative of severe deformation and typical flow instability phenomena, are closely associated with the kinked α lamellae [12]. Furthermore, Fig. 5(d3) reveals that the kinked α lamellae adjacent to the micro shear bands exhibit relatively high thermal stability during annealing.

Accordingly, this study categorizes α lamellae globularization into two distinct types, as depicted in Fig. 6: one involves splitting and recrystallization, while the other follows a shearing mechanism.

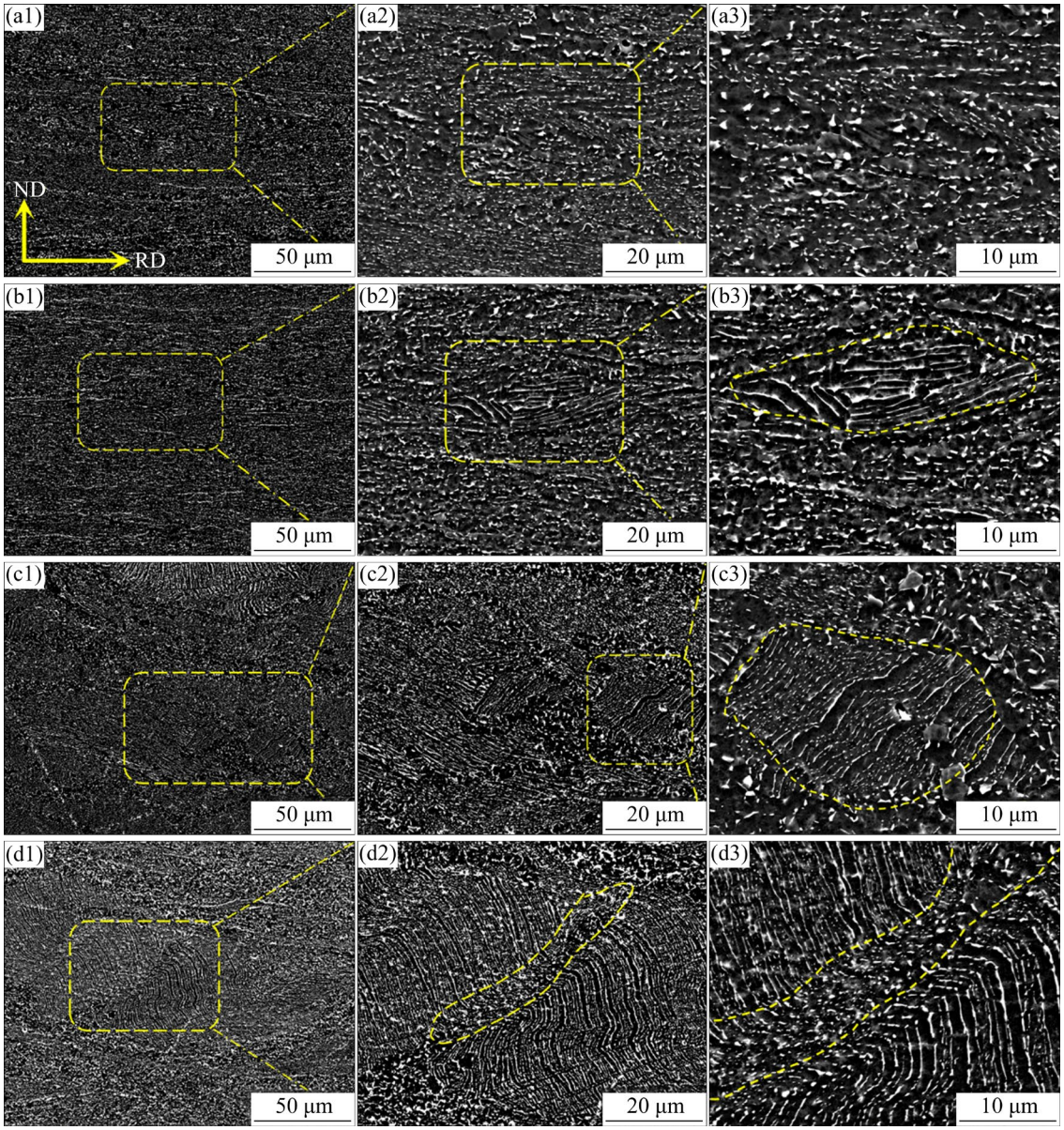

Fig. 5 SEM images of samples annealed at 700 °C for 1 h : (a1, a2, a3) RA600; (b1, b2, b3) RA700; (c1, c2, c3) RA800; (d1, d2, d3) RA900

3.2 Phase constitution

Figure 7(a) shows the XRD results for specimens rolled at temperatures ranging from 600 to 900 °C (R600 to R900). The ratio of the intergrated intensity of the $(10\bar{1}0)_{\alpha}$ peak to one of the $(110)_{\beta}$ peak was used to evaluate the volume fraction of the phase ratio, confirming a variation in the β phase fraction in response to change in rolling temperature [14]. The quantitative data for the two phases are detailed in Table 2. Additionally, statistical analysis based on SEM micrographs, as shown in Fig. 7(b), corroborates the XRD results. This analysis reveals that the volume fraction of the β phase increases while the α phase fraction decreases as the rolling temperature rises.

The variations in dislocation density for α and β phases at different rolling temperatures are depicted in Fig. 7(c), with the necessary calculation parameters listed in Table 3. The dislocation density of the α phase decreases with increasing rolling temperature, whereas that of the β phase shows a corresponding increase. Moreover, the dislocation density in the β phase is several times higher than that in the α phase. This discrepancy is rationalized by the differences in dislocation activation energies between the hexagonal close-packed (hcp) α phase and the body-centered cubic (bcc) β phase.

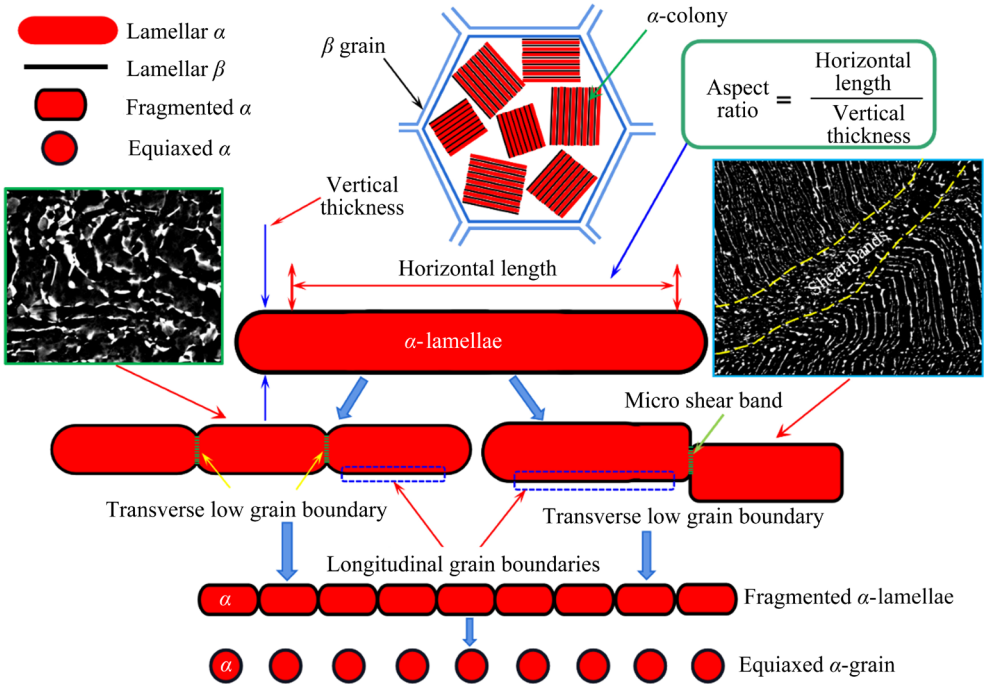

Fig. 6 Globularization mechanism from α lamellae to equiaxed α grain

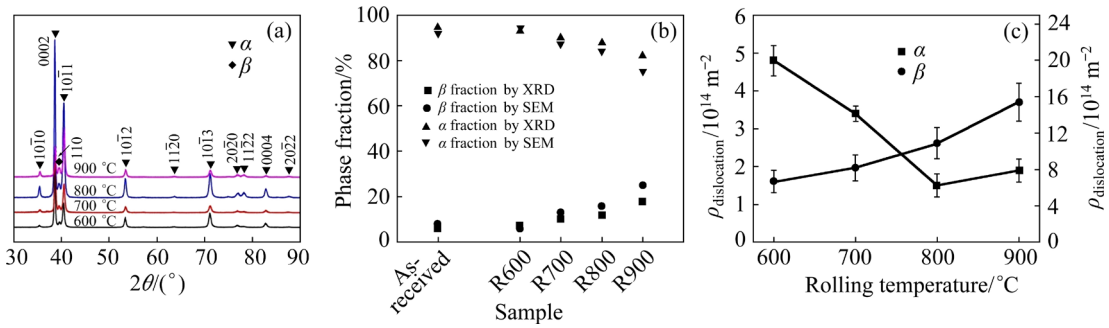

Fig. 7 XRD patterns of rolled alloy (a), phase fraction obtained from XRD and SEM (b), and dislocation densities in α and β phase (c)

Table 2 Microstructure features of rolled alloy

Sample	Phase fraction by XRD/vol.%		Phase fraction by SEM/vol.%		Width/μm	
	α	β	α	β	α	β
As-received	94±0.80	6±0.26	92±1.8	8±0.5	4±0.5	0.03±0.013
R600	93±0.63	7±0.14	94±2.9	6±0.7	2±0.5	0.08±0.023
R700	90±0.51	10±0.39	87±3.7	13±1.1	1.5±0.3	0.15±0.034
R800	88±0.32	12±0.53	84±1.3	16±1.4	1±0.2	0.2±0.043
R900	82±0.27	18±0.18	75±1.5	25±1.6	1±0.2	0.18±0.035

Table 3 Integrated intensity ratio and FWHM of diffraction peaks of rolled alloy

Sample	Integrated intensity							FWHM		Dislocation density/10^{14}m^{-2}	
	$\alpha(10\bar{1}0)$	$\alpha(0002)$	$\beta(110)$	$\alpha(10\bar{1}1)$	$\alpha(10\bar{1}2)$	$\alpha(10\bar{1}3)$	$\alpha(0004)$	$\alpha(0002)$	$\beta(110)$	α	β
R600	5.32	100	4.27	45.45	18.56	37.96	11.27	0.307	2.624	4.8	6.7
R700	7.23	100	13.738	61,87	15.73	24.296	6.80	0.291	2.732	3.4	8.2
R800	11.42	100	11.63	85.33	21.74	13.96	4.55	0.282	2.866	1.5	10.9
R900	23.01	100	22.65	192.49	36.42	44.30	17.39	0.286	2.943	1.8	15.1

3.3 EBSD analysis results of annealed alloy

Rolling deformation of the specimen entails plane strain conditions, where the specimen is elongated along the rolling direction (RD), compressed along the normal direction (ND), and remains undeformed along the transverse direction (TD). This deformation leads to physical rotation within the α-colony. In terms of slip activation, the basal $\langle a\rangle$ $\{0001\}\langle 11\bar{2}0\rangle$ and prismatic $\langle a\rangle$ $\{1\bar{1}00\}\langle 11\bar{2}0\rangle$ slips are typically activated prior to the pyramidal slip $\{10\bar{1}1\}\langle 11\bar{2}0\rangle$, due to their low and near-critical resolved shear stress (CRSS). The activation of pyramidal slip is notably more challenging due to its high CRSS and large Burgers vector [15−17].

As depicted in Fig. 8, Type III α-colonies, oriented with $\langle 0001\rangle$ along ND, present the basal (0001) plane perpendicular to the ND direction and parallel to RD. Consequently, the Schmid factor (SF) for basal slip is zero. However, certain $(10\bar{1}0)$ planes, being angled relative to RD, may permit the activation of prismatic slips. For Type I α-colonies, with $\langle 0001\rangle$ parallel to RD, the (0001) plane aligns parallel to ND and perpendicular to RD, resulting again in a SF of zero for basal slip. Nonetheless, some $(10\bar{1}0)$ planes positioned at an angle to ND can have a non-zero SF, enabling prismatic slip. In Type II α-colonies, oriented with $\langle 0001\rangle$ along the TD direction, the basal (0001) plane is parallel to the ND−RD plane, maintaining a SF of zero for basal slip. Here, prismatic slip is feasible under either ND compression or RD tension. Lastly, α-colonies in Type IV orientations, which are angled with respect to ND, RD, and TD, allow for the simultaneous activation of both prism and basal slips. Types III and II, representing hard orientations, typically become kinked during warm rolling deformation. Conversely, the remaining α-colonies in softer orientations tend to align along RD, facilitating more straightforward deformation patterns [18,19].

Specifically, the IPF map in Fig. 9(a) indicates that the unglobularized α-colony B is characterized by either c-axis//TD orientations (blue) or a closely related orientation with slight deviations (green). In Fig. 9(b) grain boundary maps reveal no intra-lamellae α/α transverse boundaries in colony B, instead, LABs are positioned along the longitudinal direction. The EBSD strain contour map in Fig. 9(c) confirms that α-colony B, being in a low strain state, represents a “hard” orientation. The kernel average misorientation (KAM) map in Fig. 9(d) further demonstrates that α-colony B has not transformed into equiaxed grains due to the absence of geometrically necessary dislocations (GNDs). Furthermore, Fig. 10(a) for RA900 illustrates that α-colonies with c-axis//ND (Type III) orientation also resist globularization and maintain lamellar morphology with a high aspect ratio. Additionally, the α lamellae within these colonies often become kinked, as circled by the dotted line, indicating a hard orientation less prone to globularization. A significant proportion of longitudinal boundaries is observed between α lamellae as shown in Fig. 10(c).

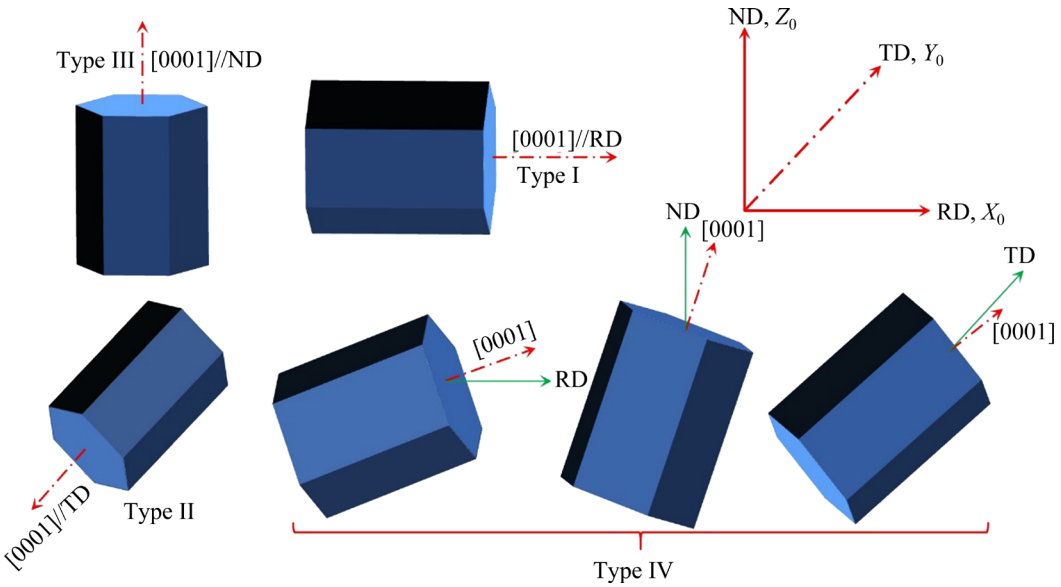

Fig. 8 Schematic showing four possible configurations of hcp α-phase according to alignment of c-axis with respect to principal direction (ND, RD and TD)

The reference colors in the IPF map (Fig. 10(a)) vary from red to magenta/violet, the latter representing a slight deviation from the red *c*-axis//ND orientation. Lastly, Fig. 10(d) highlights insufficient dislocation activity within the unglobularized α lamellae.

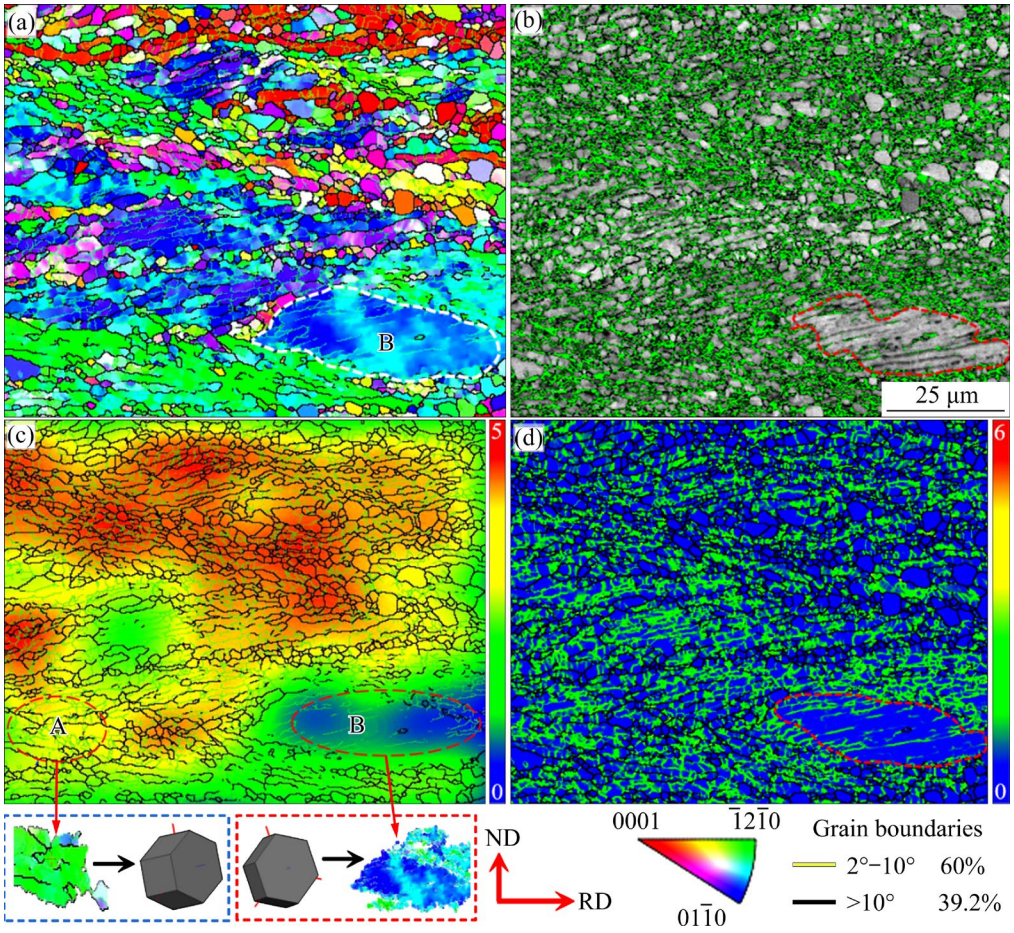

Fig. 9 IPF map of RA800 (a), grain boundary map (b), EBSD stress contour map (c), and corresponding KAM map (d)

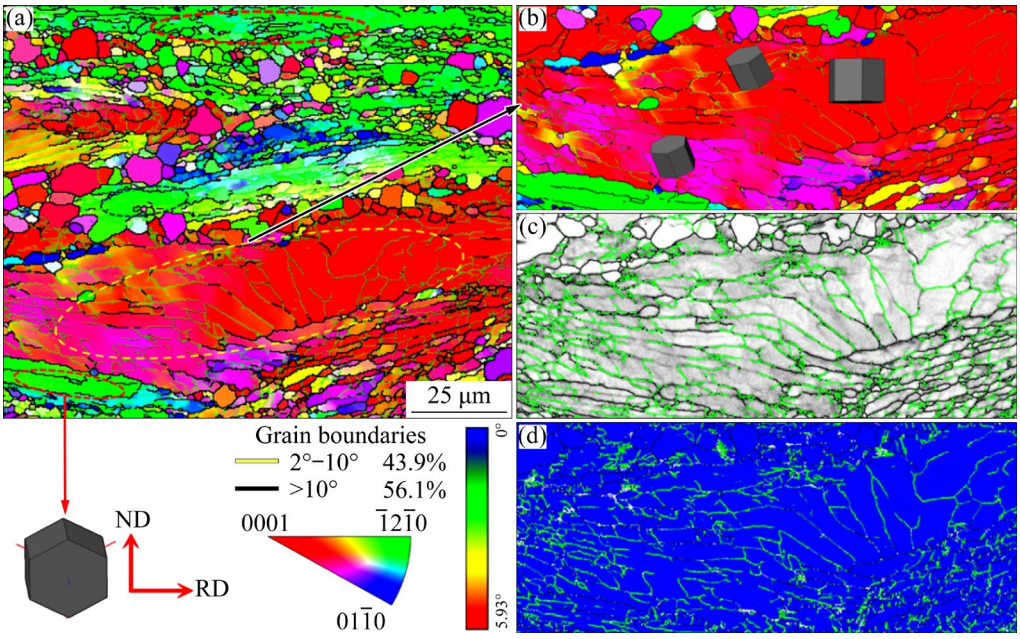

Fig. 10 IPF map of RA900 (a), partial IPF map (b) of (a), grain boundary map (c), and corresponding KAM map (d)

The IPF maps show that equiaxed α-grains exhibit a variety of orientations and encompass all possible reference colors, indicating their diverse crystallographic orientations. These spheroidized, equiaxed α-grains are more prevalent in RA600 and RA700 than in RA800 and RA900. Concurrently, many substructures or sub-grains, saturated with high-density blue LABs and termed "micro-zones" emerge, as depicted in Figs. 11(b) and (d). These equiaxed α-grains, encircled by black HABs, are indicative of their soft orientation during rolling deformation [19,20].

The heterogeneous globularization of α-colonies results in distinct sharp micro-textures, whose evolution is influenced by globularization processes, slip deformation, and phase transformations [21−23]. To further elucidate the formation mechanism of these sharp micro-textures, we analyzed the maximum micro-texture intensities presented in the pole figures (Figs. 12(b, c, d, g, h)) and correlated them with the corresponding IPF maps (Figs. 12(e, f, i, g)). Notably, the $\langle 10\bar{1}2\rangle // Z_0$ micro-texture observed in the as-received alloy stems from the $\beta \rightarrow \alpha$ phase transformation, as confirmed by the Burgers orientation relationship (BOR) depicted in Fig. 2(e). Subsequent warm heavy rolling and annealing alter the pole texture components. Clusters of globularized α grains and sub-grains, characterized by consistent crystallographic orientations, form micro-zones as shown in Figs. 12(e, f, i, g). These micro-zones exhibit varied crystal orientations, activating different slip systems that contribute to the generation of diverse sharp micro-textures during the rolling process. Due to the abundance of substructures within these micro-zones, the lamellar structure has not fully spheroidized into equiaxed grains surrounded by black HABs, as evidenced in

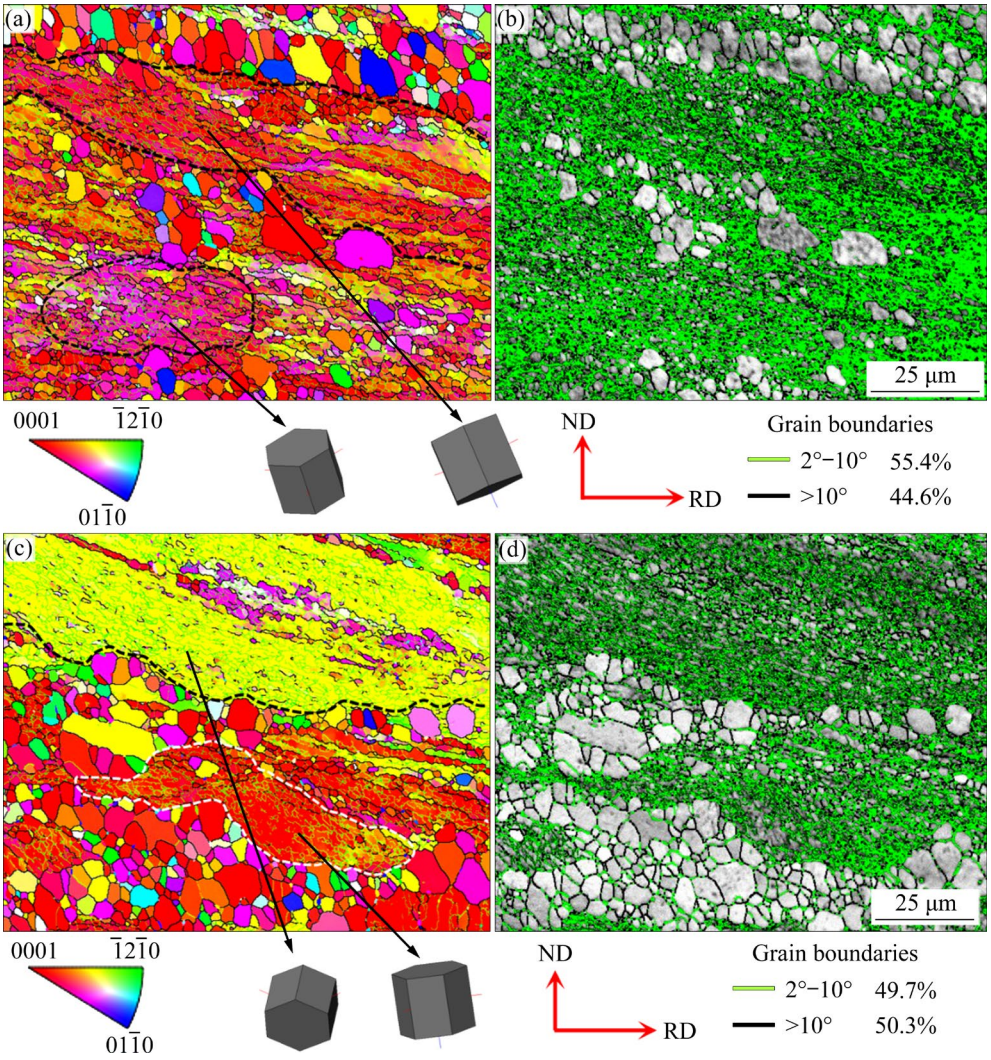

Fig. 11 IPF maps of RA600 (a) and RA700 (c), and grain boundary maps of RA600 (b) and RA700 (d)

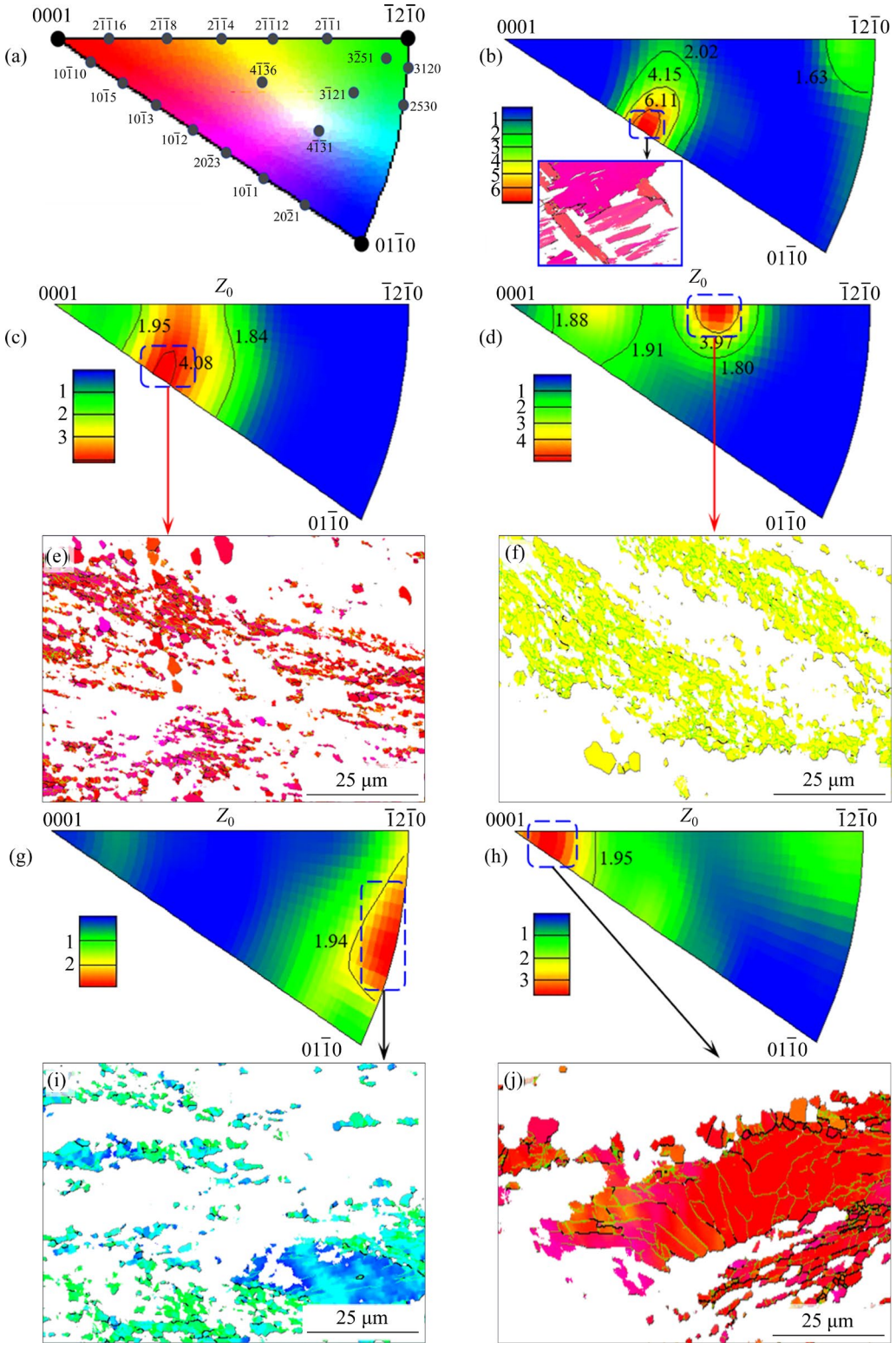

Fig. 12 Pole figures of as-received and annealed microstructure (a−d, g, h) and IPF figures corresponding to maximum texture strength (e, f, i, j): (a) Standard stereographic triangle for hcp crystal structure; (b) As-received alloy; (c, e) RA600; (d, f) RA700; (g, i) RA800; (h, j) RA900

Figs. 12(e, f). This suggests that the initial lamellar crystal orientation is relatively hard. Particularly in Fig. 12(j), kinked α lamellae with a hard crystal orientation (c-axis//ND) show resistance to globularization and exhibit a sharp texture on the pole figure. This observation underlines the critical

role of crystal orientation in influencing the microstructural responses during processing.

4 Discussion

The annealed microstructures indicate that an optimal rolling temperature for α-lamellae globularization should not be excessively high. This study identifies two primary factors contributing to the globularization fraction. First, the strain heterogeneity, stemming from crystallographic orientation differences, results in varying degrees of globularization across the microstructure. Second, higher rolling temperatures increase the β phase content, which, being softer, absorbs most of the strain during rolling deformation. This absorption by the β phase effectively reduces the globularization fraction of α phase.

4.1 Role of β phase in rolling deformation

The JMat-Pro thermodynamic calculations presented in Fig. 1(b) indicate that the equilibrium β phase content increases with temperature. Correspondingly, Fig. 7(b) shows that the β phase fraction increases with rolling temperature. The β phase, being softer, deforms more easily than the α phase. This is supported Fig. 7(c), which reveals that the dislocation density in the β phase is several times higher than that in the α phase, underscoring the significant role of β phase during rolling deformation. The deformation of the β phase results in less strain imparted to the α phase, which consequently lacks sufficient energy to develop substructures. However, the presence of transverse boundaries, composed of many substructures, is a crucial condition for the transformation of α lamellae into equiaxed grains. Therefore, as the β phase fraction increases, the globularization fraction of α lamellae decreases. Previous studies by SEMIATIN et al [24−27] suggested that the globularization of α lamellae depended on the extent of applied strain and annealing but was independent of deformation temperature between 900 and 950 °C. In contrast, our findings demonstrate that globularization of α lamellae is influenced by rolling temperature. This discrepancy is primarily due to the broad experimental temperature range considered in this study, particularly highlighting the influential role of the β phase during the rolling process.

4.2 Effect of α-colony orientation on deformation behavior

4.2.1 Slip in α-colony

Most α-colonies rotate towards the metal flow direction, facilitated by the activation of various slip systems. Thus, understanding the crystallographic rotation of these colonies is crucial. The rotation axis of α lamellae, dictated by the active slip system, can be determined using the rotation-axis equation, $w_p=a\times n$, where n is the slip plane normal, a denotes the slip direction vector, and w_p is the vector cross product of a and n [27]. In α-titanium, the prism slip system allows for lattice rotation around the [0001] direction, while the basal slip facilitates rotation around the $[10\bar{1}0]$ direction. Figure 13(a) reveals that the SF for basal $\{0001\}\langle 11\bar{2}0\rangle$ slip is 0.42. At high temperatures, the primary slip systems for α-titanium are the basal $\langle a\rangle$ slip $\{0001\}\langle 11\bar{2}0\rangle$ and the prismatic $\langle a\rangle$ slip $\{10\bar{1}0\}\langle 11\bar{2}0\rangle$ [28−32]. To accurately determine the active slip system, the SF value is combined with in-grain misorientation axis (IGMA) analysis. The intensity of IGMA around the $\langle 0001\rangle$ axis in α-colony A is 1.83, while another significant IGMA intensity around the $\langle 10\bar{1}0\rangle$ is 1.04, suggesting the co-activation of basal and prism slips during the rolling deformation of α-colony A. Despite the higher SF for basal slip, the prism slip is more effective, leading to the dominance of the $\{10\bar{1}0\}\langle 11\bar{2}0\rangle$ prism slip. Consequently, as shown in Fig. 13(c), the initial soft crystallographic orientation of α-colony A facilitates simultaneous rotation along the c-axis due to prism slip, and along the $\langle 10\bar{1}0\rangle$ direction due to basal slip.

The globularization of rolled α lamellae typically begins with boundary splitting and thermal grooving processes during annealing [33−37]. Basal slip contributes to the formation of longitudinal intra-lamellar α/α boundaries within α lamellae. Conversely, the creation of transverse α/α boundaries is primarily associated with prism slip [18,38]. However, this study further elucidates that the presence of transverse α/α boundaries, which are crucial for the globularization of α lamellae, results from the simultaneous activation of both basal and prism slips, rather than from prism slip alone.

The α-colony B, which tends to align in a Type II orientation, exhibits distinct behaviors in terms of stress state, slip activation, and globularization

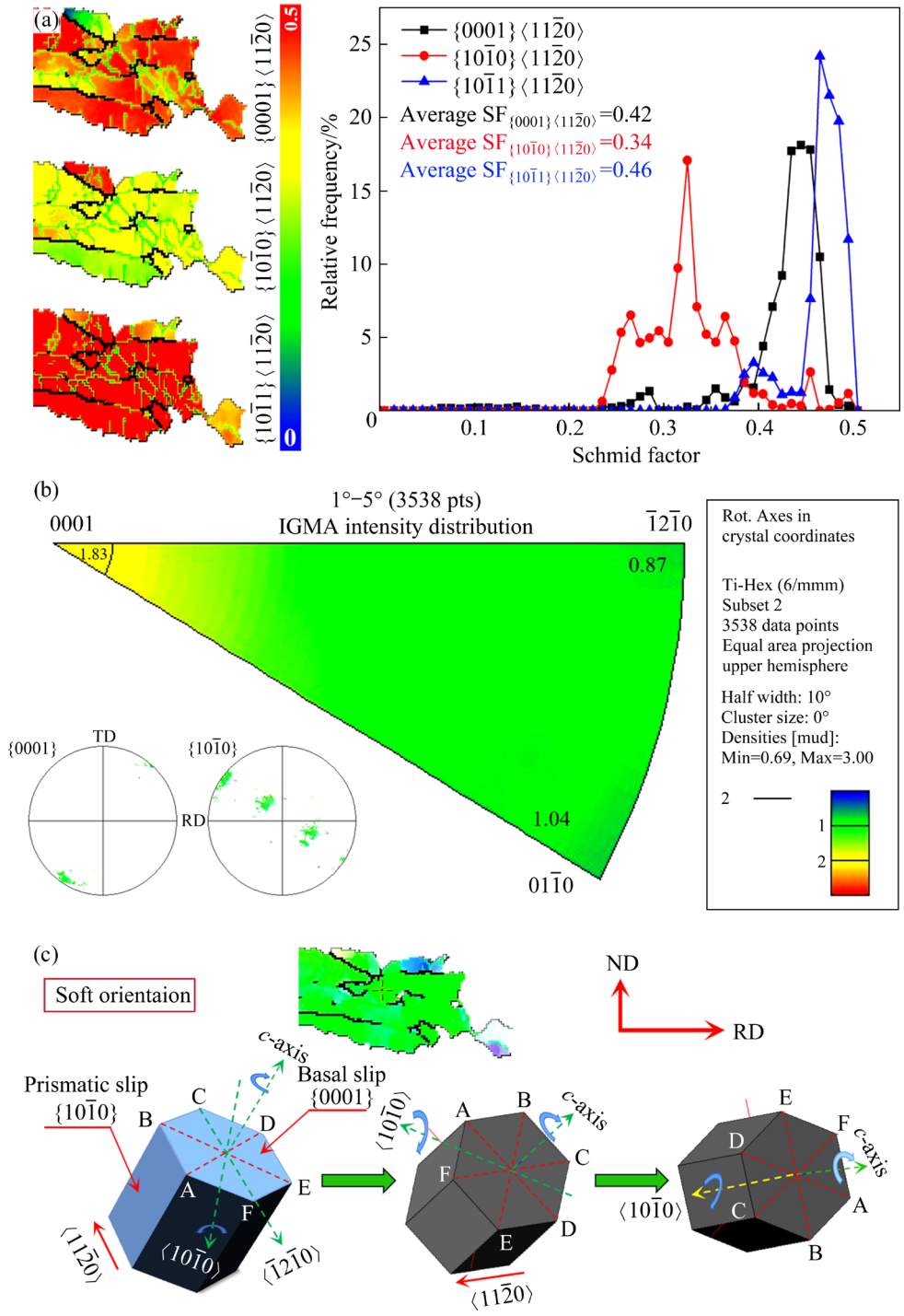

Fig. 13 SF map of α-colony A and corresponding statistics (a), IGMA distribution of α-colony A (b), and schematic diagram revealing crystallographic orientation change for α-colony A during rolling deformation (c)

extent compared to α-colony A. As indicated in Fig. 9(a), α-colony B maintains high thermal stability during annealing. The SF for prism slipping in α-colony B is 0.46, significantly higher than that for basal slip, which is only 0.2, as shown in Fig. 14(a). Furthermore, the intensity of the IGMA around the ⟨0001⟩ axis for α-colony B is notably high at 3.83, while the IGMA intensities around the ⟨10$\bar{1}$0⟩ and ⟨uvto⟩ are negligible, as depicted in Fig. 14(b). This suggests that prism slip is predominantly active during the rolling deformation of α-colony B, leading to rotation of the hcp unit cell about the c-axis under the influence of prism slip, as further demonstrated in

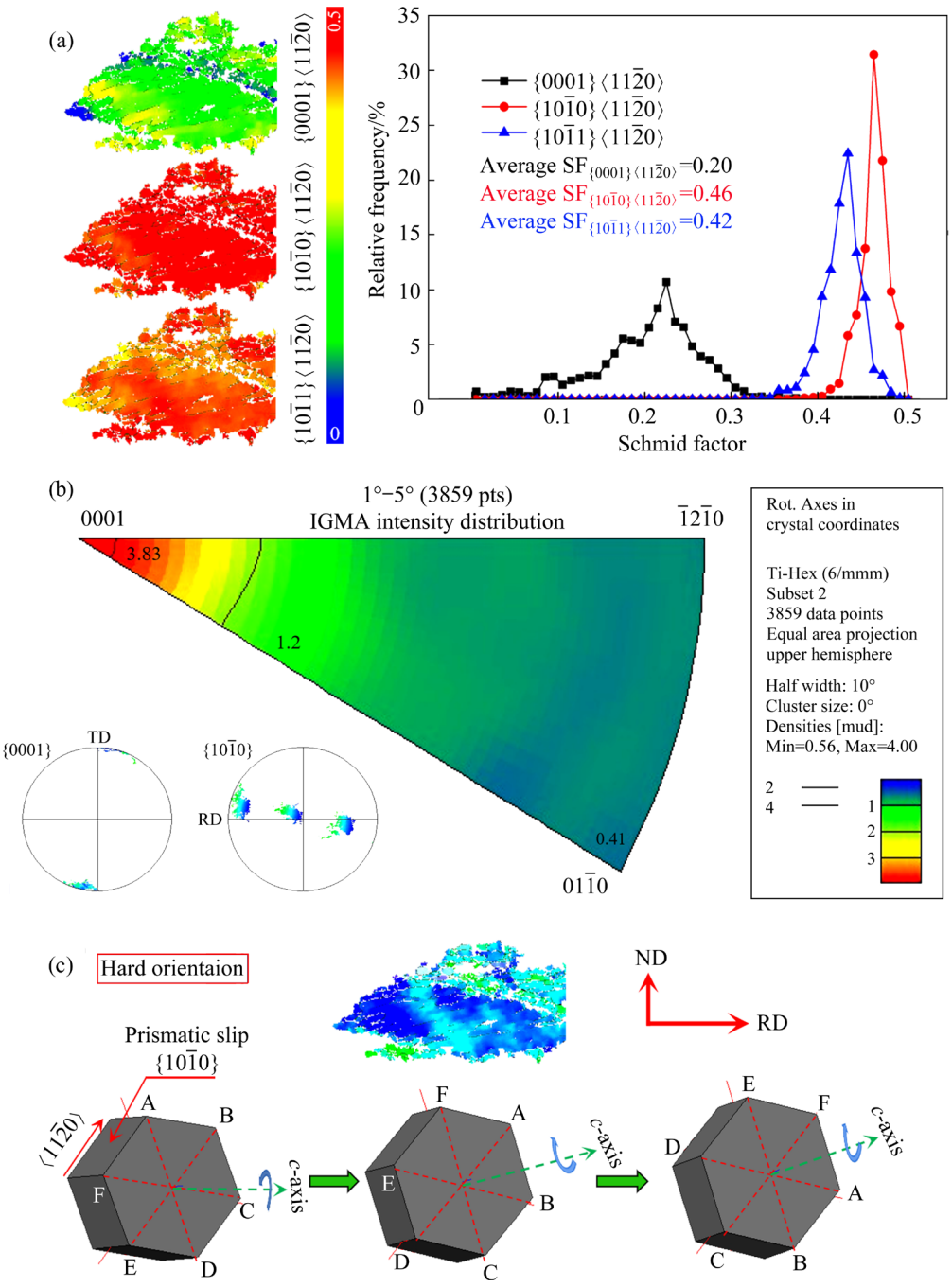

Fig. 14 SF map of α-colony B and corresponding statistics (a), IGMA distribution for α-colony B (b), and schematic diagram revealing crystallographic orientation change for α-colony B during rolling deformation (c)

Fig. 14(c). Additionally, Fig. 9(b) reveals the absence of transverse α/α boundaries within α lamellae in colony B, with only a few longitudinal intra-lamellar α/α boundaries present. This observation leads to the conclusion that the activation of solely prism $\langle a \rangle$ slip in α-colony B is insufficient to promote the formation of transverse intra-lamellar α/α boundaries. Consequently, the globularization rate of α-colony B is markedly slower compared to α-colony A.

4.2.2 Kinking of α-colony

In the orientation of kinked α-colonies, where ND aligns with $\langle 0001 \rangle$ as shown in Fig. 10(b), these colonies resist compression in the ND direction and extend along the RD direction, facilitated by limited prism slip. Under rolling strain, some of these hard α-colonies rotate towards the RD direction, while others maintain their initial orientation. This differential behavior results in localized material flow within certain microstructural regions of the

α-colonies, leading to the formation of micro shear bands across these regions, as depicted in Fig. 5(d3). These shear bands contribute to further rotational transformations of the α-colonies on either side, causing the initial orientation to gradually shift to another that deviates from ND//⟨0001⟩. The deviated orientation, represented by violet in the IPF map, is adjacent to the red-colored α-colonies, as visible in Fig. 10. MIROOV et al [27] described a similar β Zigzag behavior and attributed this phenomenon to the extension of micro shear bands over the entire α-colony. Likewise, Fig. 10(a) shows some boundary segments outlined by LABs becoming slightly bent with Zigzag distortions, indicating the progressive development of shear bands and localized severe plastic deformation.

Figures 15(b, d) indicate that the SF for prism slip in kinked α-colonies is 0.42, significantly higher than that for basal slip, while the activation of pyramidal slip remains limited due to its high CRSS, even at elevated temperatures such as 900 °C [3,39]. Consequently, at a rolling temperature of 900 °C, deformation in kinked α-colonies predominantly occurs through prismatic

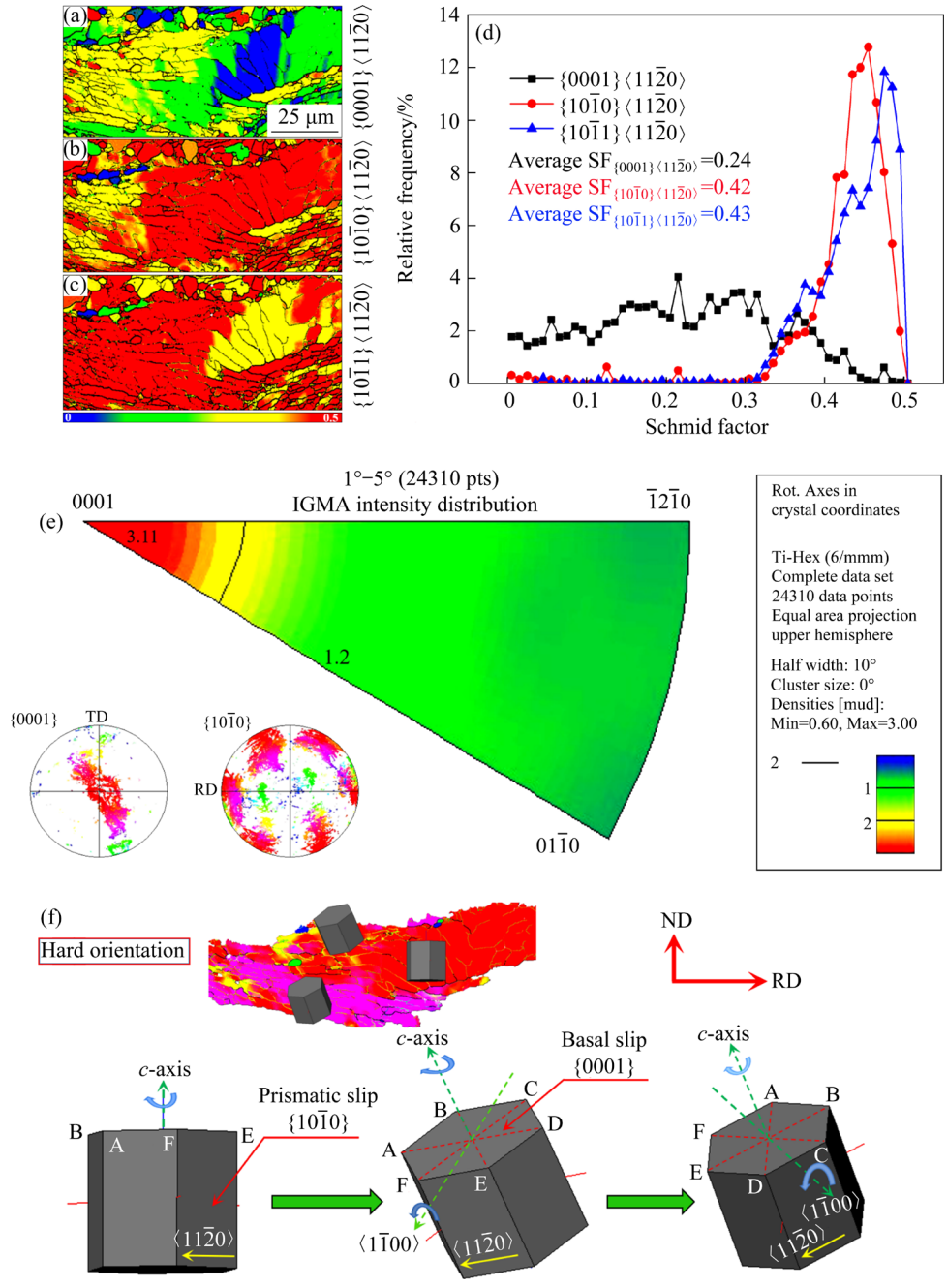

Fig. 15 SF map of kinked α-lamella and corresponding statistics (a, b, c, d), IGMA distribution of kinked α-colony (e), and schematic diagram of crystallographic orientation changes for kinked α-colony during rolling deformation (f)

slip. This is corroborated by the intensity of the IGMA around the ⟨0001⟩ axis being 3.11 (Fig. 15(e)), which is substantially higher than those around ⟨10$\bar{1}$0⟩ and ⟨uvto⟩, indicating that the crystal lattice of kinked α-colonies rotates along the ⟨0001⟩ axis under prism slip. However, the IGMA intensity around the ⟨0001⟩ axis is more dispersed compared to that shown in Fig. 14(b). Additionally, Fig. 15(f) reveals a slight rotation of the crystallographic orientation of kinked α-colonies along the ⟨1$\bar{1}$00⟩ direction, suggesting a minor contribution from basal slip to the kinking deformation. The activation of basal slip is largely due to the rotation of α-colonies during warm rolling deformation, as the angle between the c-axis and the deformation direction increases, so does the SF on the basal plane. However, given the limited effect of basal slip, longitudinal intra-lamellar α/α boundaries are more prevalent than transverse ones.

Due to these factors, kinked α-colonies face challenges in globularizing through boundary splitting and thermal grooving, making their transformation less likely compared to other orientations.

4.2.3 Development of local misorientation within individual α-colony

Figure 16(a) displays the IPF map of an unglobularized α-colony along with its corresponding misorientation profiles along the dotted read line, as shown in Fig. 16(b). The cumulative misorientation profile illustrates both continuous smooth changes and discontinuous changes in orientation evolution along α lamellae. Notably, at Point 1 on the IPF map, where the orientation change is discontinuous, the point-to-point misorientation remains below 5°. Figure 16(c) visualizes the misorientation formation within α-colony A. Previous studies [20,26,40] have suggested that a point-to-point misorientation of at least 5° is required for boundary formation during annealing. The analysis from Fig. 14 indicates that the minor misorientation within α-colony B is primarily a result of the rotation of the hcp unit cell around the ⟨0001⟩ direction. Thus, it can be concluded that the activation of a single prismatic slip is insufficient to produce transverse boundaries necessary for completing the globularization of α-colonies. However, the discontinuous change

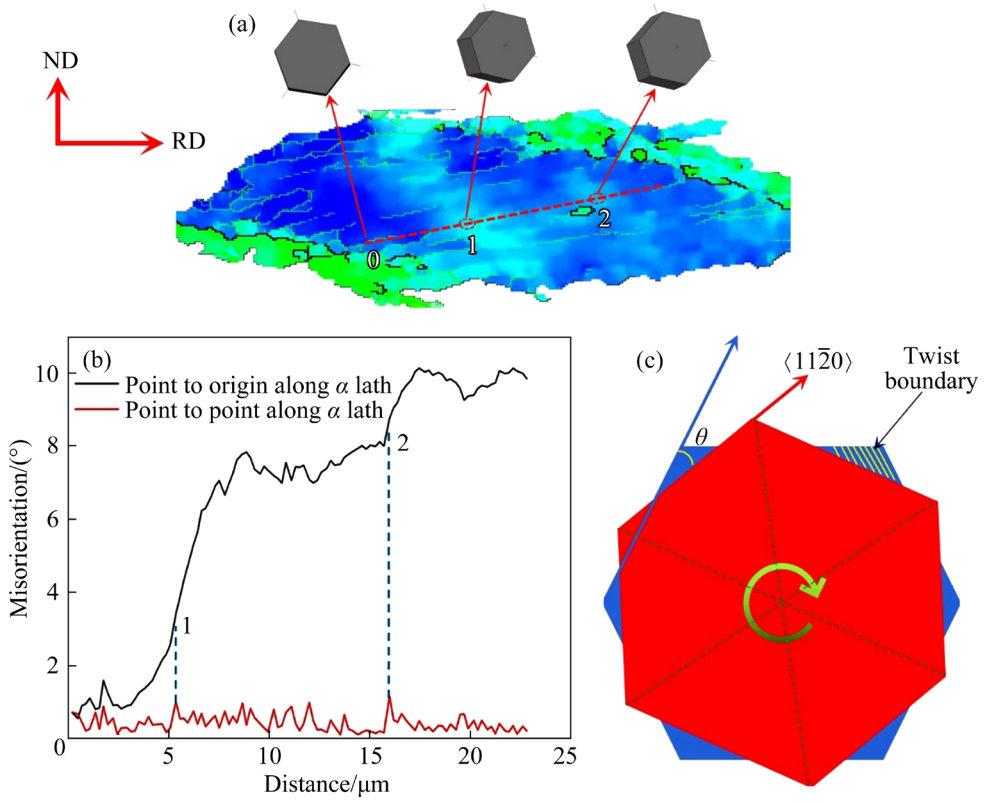

Fig. 16 IPF map with overlaid unit cell of α-colony A (a), misorientation profiles along line 0−2 (cumulative misorientation profile along line relative to orientation at point 0, and point-to-point misorientation profile along line) (b), and misorientation formation in α-colony A (c)

observed at Point 1 in Fig. 16(a) suggests that this location is more conducive to the formation of high-angle α/α boundaries compared to other points, providing a potential site for enhanced boundary development.

Figure 17(a) illustrates the misorientation evolution associated with the kinked α-colony. IGMA analysis, when integrated with SF maps, reveals that the hexagonal unit cell corresponding to this kinked α-colony microstructure undergoes rotation along the c-axis due to the activation of prism slip. The cumulative misorientation profile depicted in Fig. 17(b) identifies discontinuous change points labeled A, B, C, D, E, and F, which have transitioned into grain boundaries. Notably, the point-to-point misorientations at points A, B, C, D and E exceed 5° but remain below 10°, resulting in the formation of blue LABs, whereas the misorientation at Point F exceeds 10°, leading to the formation of black HABs. Despite the significant misorientation sufficient to foster both LABs and, in the case of Point F, these HABs manifest as longitudinal intra-lamellar α/α boundaries, rather than the more transformative transverse α/α boundaries. Consequently, the globularization of the kinked α-colony proceeds sluggishly. Moreover, the misorientation values observed in the kinked α-colony are greater than those in the unglobularized α-colony B referenced in Fig. 16(a). This increased misorientation is attributed not only to the rotation along the c-axis under prism slip but also to a slight rotation along the $\langle 10\bar{1}0\rangle$ direction under basal slip, as indicated in Fig. 15. These results suggest that a relatively high misorientation, arising from the co-activation of both prism and basal slips within the α-colony, is essential to achieve complete globularization.

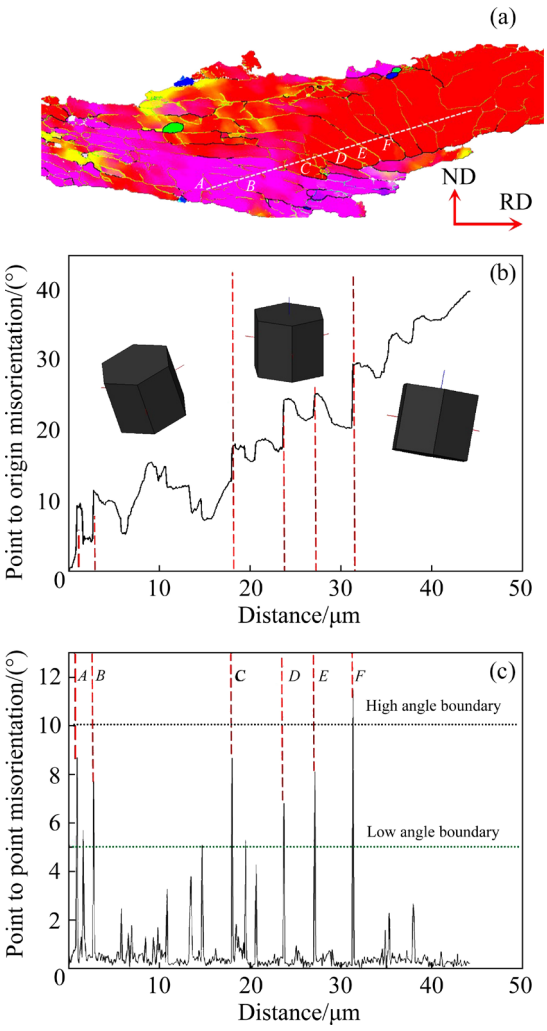

Fig. 17 IPF map with overlaid unit cell of kinked α-colony (a), and misorientation profiles along lines A−F (cumulative misorientation profile along line relative to orientation at Point A, and point-to-point misorientation profile along line) (b, c)

5 Conclusions

(1) Globularization of α-lamellae during static annealing is significantly influenced by rolling temperature. Rolling at 600 and 700 °C is found to be more effective than at 800 and 900 °C.

(2) The α-colonies with soft orientations, angled relative to ND, RD and TD, can activate both basal and prism slips, facilitating the formation of critical intra-lamellar α/α transverse boundaries essential for globularization. Conversely, colonies with hard orientations, such as $\langle 0001\rangle$//ND or $\langle 0001\rangle$//TD, predominantly activate the prism slip system. Specifically, α-colonies with $\langle 0001\rangle$//ND orientation become kinked during rolling and maintain a high aspect ratio after annealing, leading to sluggish globularization.

(3) The globularization of α-colonies is inherently heterogeneous, influenced by their crystal orientation. The emergence of micro-zones displays sharp α textures in pole figures, predominantly linked to the hard primitive crystal orientation of the α-colonies.

(4) Misorientation within α-colonies arises from hexagonal close-packed (hcp) crystal rotation during rolling deformation. Substantial misorientation resulting from the co-activation of prism and basal slips can produce sufficient

misorientation to generate LABs necessary for complete globularization.

CRediT authorship contribution statement

Xiao-feng WU: Conceptualization, Methodology, Software, Data curation, Writing − Original draft; **Li-ming FU:** Supervision, Project administration, Data curation; **Shuo MA:** Investigation, Formal analysis, Validation; **Ai-dang SHAN:** Investigation, Resources, Data curation.

Declaration of competing interest

The authors declare that they have no known competing financial interests or personal relationships that could have appeared to influence the work reported in this paper.

References

[1] ZHANG Jian, LI Hong-wei, ZHAN Mei. Review on globularization of titanium alloy with lamellar colony [J]. Manufacturing Review, 2020, 7: 18.

[2] GAO Peng-fei, FU Ming-wang, ZHAN Mei, LEI Zhen-ni, LI Yan-xi. Deformation behavior and microstructure evolution of titanium alloys with lamellar microstructure in hot working process: A review [J]. Journal of Materials Science & Technology. 2020, 39: 58−75.

[3] WANG Ke, WU Ming-yu, REN Zhao, ZHANG Yu, XIN Ren-long, LIU Qing. Static globularization and grain morphology evolution of α and β phases during annealing of hot-rolled TC21 titanium alloy [J]. Transactions of Nonferrous Metals Society of China, 2021, 31(9): 2664−2676.

[4] SEMIATIN S L. An overview of the thermomechanical processing of α/β titanium alloys: Current status and future research opportunities [J]. Metallurgical and Materials Transactions A, 2020, 51: 2593−2625.

[5] JIANG Xue-qi, FAN Xiao-guang, LI Qi. ZHAN Mei. Strengthened flow instability in hot deformation of titanium alloy with colony structure: On the effect of microstructure heterogeneity [J]. Journal of Alloys and Compounds, 2019, 801: 381−393.

[6] JIA Zhi-qiang, XU Jian-wei, ZENG Wei-dong, SUN Xin, ZHOU Jian-hua. Static globularization kinetics for Ti-17 alloy with initial lamellar microstructure [J]. Journal of Alloys and Compounds, 2014, 603: 239−247.

[7] BIELER, T R, SEMIATIN S L. The origins of heterogeneous deformation during primary hot working of Ti−6Al−4V [J]. International Journal of Plasticity, 2002, 18: 1165−1189.

[8] ZHAO Zi-bo, WANG Qing-jiang, HU Qing-miao, LIU Jian-rong, YU Bing-bing, YANG Rui. Effect of β(110) texture intensity on α-variant selection and microstructure morphology during $\beta\rightarrow\alpha$ phase transformation in near α titanium alloy [J]. Acta Materialia, 2017, 126: 372−382.

[9] WU Cheng-bao, YANG He, FAN Xiao-guang, SUN Zhi-chao. Dynamic globularization kinetics during hot working of TA15 titanium alloy with colony microstructure [J]. Transactions of Nonferrous Metals Society of China, 2011, 21: 1963−1969.

[10] ROY S, KARANTH S, SUWAS S. Microstructure and texture evolution during sub-transus thermo-mechanical processing of Ti−6Al−4V−0.1B alloy: Part II. Static annealing in (α+β) regime [J]. Metallurgical and Materials Transactions A, 2013, 44: 3322−3336.

[11] SHARMA G, RAMANUJAN R V, TIWARI G P. Instability mechanisms in lamellar microstructures [J]. Acta Materialia, 2000, 48: 875−889.

[12] UNGÁR T, BALOGH L, RIBÁRIK G. Defect-related physical-profile-based X-ray and neutron line profile analysis [J]. Metallurgical and Materials Transactions A, 2010, 41: 1202−1209.

[13] LI Hong-jia, CAI Wu-peng. Understanding the deformation mechanism of individual phases of a dual-phase beta type titanium alloy using in situ diffraction method [J]. Materials Science and Engineering: A, 2018, 728: 151−156.

[14] DRAGOMIR I C, LI D S, CASTELLO-BRANCO G A, GARMESTANI H, SNYDER R L, RIBARIK G, UNGAR T. Evolution of dislocation density and character in hot rolled titanium determined by X-ray diffraction [J]. Materials Characterization, 2005, 55: 66−74.

[15] ZAEFFERER S. A study of active deformation systems in titanium alloys: Dependence on alloy composition and correlation with deformation texture [J]. Materials Science and Engineering: A, 2003, 344: 20−30.

[16] GROVES G W, KELLY A. Independent slip systems in crystals [J]. Philosophical Magazine, 1963, 8: 877−887.

[17] YOO M H. Slip, twinning, and fracture in hexagonal close-packed metals [J]. Metallurgical and Materials Transactions A, 1981, 12: 409−418.

[18] ROY S, SUWAS S. Orientation dependent spheroidization response and macro-zone formation during sub β-transus processing of Ti−6Al−4V alloy [J]. Acta Materialia, 2017, 134: 283−301.

[19] WANG Li, FAN Xiao-guang, ZHAN Mei. JIANG Xue-qi, ZENG Xiang, LIANG Yong-feng, ZHENG Huo-jun, ZHAO An-ming. The heterogeneous globularization related to crystal and geometrical orientation of two-phase titanium alloys with a colony microstructure [J]. Materials & Design, 2020, 186: 108338.

[20] ZHAO Zhi-bo, WANG Qing-jiang, LIU Jian-rong, YANG Rui. Characterizations of microstructure and crystallographic orientation in a near-α titanium alloy billet [J]. Journal of Alloys and Compounds, 2017, 712: 179−184.

[21] ZHENG Guo-ming, MAO Xiao-nan, TANG Bin, ZHANG Yong-qiang. Evolution of microstructure and texture of a near α titanium alloy during forging bar into disk [J]. Journal of Alloys and Compounds, 2020, 831: 154750.

[22] GERMAIN L, GEY N, HUMBERT M, VO P, JAHAZI M, BOCHER P. Texture heterogeneities induced by subtransus processing of near α titanium alloys [J]. Acta Materialia, 2008, 56: 4298−4308.

[23] GEY N, BOCHER P, UTA E, GERMAIN L, HUMBERT M. Texture and microtexture variations in a near-α titanium forged disk of bimodal microstructure [J]. Acta Materialia, 2012, 60: 2647−2655.

[24] SHELL E B, SEMIATIN S L. Effect of initial microstructure on plastic flow and dynamic globularization during hot working of Ti−6Al−4V [J]. Metallurgical and Materials Transactions A, 1999, 30: 3219−3229.

[25] STEFANSSON N, SEMIATIN S L, EYLON D. The kinetics of static globularization of Ti−6Al−4V [J]. Metallurgical and Materials Transactions A, 2002, 33: 3527−3534.
[26] STEFANSSON N, SEMIATIN S L. Mechanisms of globularization of Ti−6Al−4V during static heat treatment [J]. Metallurgical and Materials Transactions A, 2003, 34: 691−698.
[27] MIRONOV S, MURZINOVA M, ZHEREBTSOV S, SALISHCHEV G A, SEMIATIN S L. Microstructure evolution during warm working of Ti−6Al−4V with a colony-α microstructure [J]. Acta Materialia, 2009, 57: 2470−2481.
[28] ZHEREBTSOV S, MURZINOVA M, SALISHCHEV G, SEMIATIN S L. Spheroidization of the lamellar microstructure in Ti−6Al−4V alloy during warm deformation and annealing [J]. Acta Materialia, 2011, 59: 4138−4150.
[29] SEMIATIN S L, SEETHARAMAN V, WEISS I. Flow behavior and globularization kinetics during hot working of Ti−6Al−4V with a colony alpha microstructure [J]. Materials Science and Engineering: A, 1999, 263: 257−271.
[30] RAPPERPORT E J, HARTLEY C S. Deformation modes of zirconium at 77, 575, and 1075 K [J]. Transactions of the Metallurgical Society of AIME, 1960, 218: 869−876.
[31] CHUN Y B, BATTAINI M, DAVIES C H J, HWANG S K. Distribution characteristics of in-grain misorientation axes in cold-rolled commercially pure titanium and their correlation with active slip modes [J]. Metallurgical and Materials Transactions A, 2010, 41: 3473−3487.
[32] LI Nan, ZHAO Zhi-bo, ZHU Shao-xiang, ZHOU Tian-ya, WANG Qi-jiang, SUN Hao, LIU Yuan-hong. Analysis of the active slip mode during compression of the near-α titanium alloy in the α+β phase-field: Insights from the results of electron backscattered diffraction [J]. Materials Letters, 2021, 288: 129363.
[33] CHEN Ke, LUO Jiao, HAN Wen-chao, LI Miao-quan. Formation and evolution of new α grain boundary and its influence on globularization of α lamellae in TC17 alloy [J]. Journal of Alloys and Compounds, 2020, 848: 156141.
[34] ZHAO Peng-yang, SHEN Chen, SAVAGE M F, Li Ju, NIEZGODA S R, MILLS M J, WANG Yun-zhi. Slip transmission assisted by Shockley partials across α/β interfaces in Ti-alloys [J]. Acta Materialia, 2019, 171: 291−305.
[35] CHONG Yan, BHATTACHARJEE T, TSUJI N. Bi-lamellar microstructure in Ti−6Al−4V: Microstructure evolution and mechanical properties [J]. Materials Science and Engineering: A, 2019, 762: 138077.
[36] SALEM A A, SEMIATIN S L. Anisotropy of the hot plastic deformation of Ti−6Al−4V single-colony samples [J]. Materials Science and Engineering: A, 2009, 508: 114−120.
[37] GAO Peng-fei, ZHAN Mei, FAN Xiao-guang, LEI zhen-ni, CAI Yang. Hot deformation behavior and microstructure evolution of TA15 titanium alloy with nonuniform microstructure [J]. Materials Science and Engineering: A, 2017, 689: 243−251.
[38] SINGH G, FONSECA J Q D, PREUSS M. Microstructure evolution and deformation texture during rolling of TIMETAL ®407 [J]. Materialia, 2020, 9: 100596.
[39] WEISS I, FROES F H, EYLON D, WELSCH G E. Modification of alpha morphology in Ti−6Al−4V by thermomechanical processing [J]. Metallurgical and Materials Transactions A, 1986, 17: 1935−1947.
[40] ITO Y, MURAKAMI S, TSUJI N. SEM/EBSD analysis on globularization behavior of lamellar microstructure in Ti−6Al−4V during hot deformation and annealing [J]. Metallurgical and Materials Transactions A, 2017, 48: 4237−4246.

Ti−6Al−4V 合金片层组织在大变形温轧以及退火过程中的不均匀球化

武晓峰[1]，付立铭[1,2,3]，马 硕[1,2]，单爱党[1,2,3]

1. 上海交通大学 材料科学与工程学院，上海 200240；
2. 上海交通大学 高温材料精密成型上海重点实验室，上海 200240；
3. 先进船舶与深海研究联合创新中心，上海 200240

摘 要：研究轧制温度和 α 晶体取向对 Ti−6Al−4V 合金中 α+β 片层组织球化的影响。首先，将片层组织分别在 600、700、800 和 900 ℃下进行大变形轧制。在 600~900 ℃的轧制温度范围内，β 相的体积分数和片层厚度随轧制温度的升高而增加，而 α 相的体积分数和片层厚度随轧制温度的升高而降低。轧制后的片层组织在退火过程中通过球化转变为等轴晶。结果表明，片层组织的球化分数随轧制温度的升高而降低。此外，轧制后的 α 片层组织在退火过程中具有硬取向(〈0001〉//ND 和〈0001〉//TD）片层的球化率低于具有软取向(分别与 ND、RD 和 TD 呈一定角度)片层的球化率。片层组织的不均匀球化将导致一些强织构微区产生。 此外，详细阐述具有不同晶体取向的 α 片层组织在轧制过程中的滑移变形行为。

关键词：不均匀球化；Ti−6Al−4V 合金；片层组织；滑移；取向；取向差

(Edited by Xiang-qun LI)